Robust phase recovery in temporal speckle pattern interferometry using a 3D directional wavelet transform

Alejandro Federico[1,*] and Guillermo H. Kaufmann[2]

[1]*Electrónica e Informática, Instituto Nacional de Tecnología Industrial, P.O. Box B1650WAB, B1650KNA San Martín, Argentina*

[2]*Instituto de Física Rosario and Centro Internacional Franco Argentino de Ciencias de la Información y de Sistemas, Boulevard 27 de Febrero 210 bis, S2000EZP Rosario, Argentina*

**Corresponding author: federico@inti.gov.ar*

Received May 12, 2009; revised June 17, 2009; accepted June 23, 2009; posted July 13, 2009 (Doc. ID 111309); published July 27, 2009

We propose an approach based on a 3D directional wavelet transform to retrieve optical phase distributions in temporal speckle pattern interferometry. We show that this approach can effectively recover phase distributions in time series of speckle interferograms that are affected by sets of adjacent nonmodulated pixels. The performance of this phase retrieval approach is analyzed by introducing a temporal carrier in the out-of-plane interferometer setup and assuming modulation loss and noise effects. The advantages and limitations of this approach are finally discussed. © 2009 Optical Society of America

OCIS codes: 120.6165, 120.5050.

Temporal speckle pattern interferometry (TSPI) is a well-established technique for measuring dynamic displacement fields produced by diffusely reflecting objects (see [1] and references therein). In TSPI, the displacement of the rough object produces intensity modulations at all pixels belonging to the recorded time series of speckle interferograms. The sequential acquisition of a large number of speckle interferograms and its postprocessing facilitate the recovery of the phase distribution, so that the whole-field dynamic displacement field can be determined. In this framework, the phase distribution is commonly recovered using a temporal phase shifting algorithm, and the unwrapping is performed as a function of time. As temporal phase unwrapping involves only 1D signals, this procedure is generally much easier to carry out, and the implementation of more complex phase unwrapping procedures is avoided. The weakness of TSPI lies in its low tolerance to unwanted effects, such as nonmodulated pixels, modulation loss, and noise, which make more difficult the phase recovery process. Therefore one of the key issues in TSPI is the development of more robust phase recovery approaches.

Currently, 1D time-frequency phase retrieval methods based on the application of the continuous wavelet transform (CWT) are widely used (see [2–4] and references therein). More recently, techniques based on a combination of the Fourier transform and the CWT [5], the empirical mode decomposition and the Hilbert transform (HT) [6], and the generalized S-transform (GST) [7] have also been developed. In [7] it was shown that the GST is better adapted to the phase recovery problem than the approaches based on the CWT, the HT, and smooth time-frequency distributions. However, these time-frequency analyses fail when a significant number of sets of adjacent nonmodulated pixels are present in the recorded data. Clearly, this problem is extremely difficult to solve by using these techniques, because the information is absent in the pixel set.

In this Letter we show that this limitation can be significantly overcome by considering the information in the neighborhood of the modulated pixels (e.g., see references [1,8]), and that for this purpose the application of a 3D approach is a valuable tool. Here we propose the use of a 3D directional wavelet transform (3DDWT) that is robust and therefore enhances the process of phase unwrapping. Thus the application of commonly used 1D unwrapping techniques are appropriated. Below we briefly discuss the characteristics of the 3DDWT and also present the obtained improvements in TSPI when the proposed technique is applied.

A 3D wavelet is a square-integrable complex-valued function $\psi(\mathbf{x})$ with zero mean that is well localized both in position and in spatial frequency spaces. The 3D directional wavelet transform $S(a,\theta,\zeta,\mathbf{b})$ of the intensity $I(\mathbf{x})$, $\mathbf{x}=(x_1,x_2,x_3)\in\mathbb{R}^3$, where $\mathbb{R}$ denotes the set of real numbers, is defined as [9]

$$S(a,\theta,\zeta,\mathbf{b}) = C_\psi \frac{1}{a}\int \mathrm{d}^3\mathbf{x}\,\psi^*\left[\frac{1}{a}r_{-\theta\zeta}(\mathbf{x}-\mathbf{b})\right]I(\mathbf{x}), \quad (1)$$

where $(^*)$ denotes complex conjugation, $a>0\in\mathbb{R}$ is the dilation parameter, $\mathbf{b}\in\mathbb{R}^3$ is the displacement parameter, C_ψ is a normalization constant, and $r_{-\theta\zeta}$ acts as a rotation operator with θ around the x_3 axis and ζ around the x_2 axis. Note that the wavelet $\psi(a,\theta,\zeta,\mathbf{x})$ is translated by $\mathbf{b}$, rotated by (θ,ζ), and dilated by the scale a. Equation (1) is a convolution with a zero-mean function $\psi(a,\theta,\zeta,\mathbf{x})$, so that $S(a,\theta,\zeta,\mathbf{b})$ acts on the intensity $I(\mathbf{x})$ as a local filter in all variables: a, θ, ζ, and $\mathbf{b}$. Therefore $S(a,\theta,\zeta,\mathbf{b})$ has an appreciable

0146-9592/09/152336-3/$15.00

value only where it matches the features of the local intensity.

We consider the TSPI signal as represented by the intensity $I(n_x,n_y,t_n)$ that is measured by a CCD detector at a specific pixel (n_x,n_y) at time t_n. Owing to the symmetry imposed by the introduction of the temporal carrier, here we propose $\theta=0$, $\zeta=0$; therefore $r_{-\theta\zeta}$ is the identity operator, and the following modified Morlet wavelet is the analyzing wavelet:

$$\psi(x,y,t) = e^{ik_0 t/\sigma_t} e^{-[(x/\sigma_x)^2+(y/\sigma_y)^2+(t/\sigma_t)^2]/2}, \qquad (2)$$

where $(\sigma_x,\sigma_y,\sigma_t)\in\mathbb{R}^3$ are the parameters of anisotropy and $k_0=2\pi$. Usually, a correction term must be added in Eq. (2) to enforce the admissibility condition, although this addition is numerically negligible for $k_0\geqslant 2\pi$. Note that in the Fourier space representation, the Fourier transform of Eq. (2) is a convex cone centered at k_0. Therefore the angular selectivity can be incremented with the increase of the anisotropy, and a better performance can be selected. To obtain a practical insight of the proposed approach, we can replace Eq. (2) in Eq. (1) and arrange the terms by identifying the 2D spatial Gaussian dependence $\psi_G(x,y)$ and the 1D temporal Morlet wavelet $\psi_M(t)$. Therefore the 3DDWT can be seen as a spatial convolution of the temporal intensity frames with a 2D Gaussian function, and the CWT of the temporal history in each spatially convolved pixel by using the Morlet wavelet,

$$S(a,x,y,t) = C_\psi \frac{1}{a}\int \mathrm{d}t'\,\psi_M^*\left[\frac{1}{a}(t'-t)\right] \times \int\int \mathrm{d}x'\mathrm{d}y'\,\psi_G \times \left[\frac{1}{a}(x'-x,y'-y)\right] I(x',y',t'). \qquad (3)$$

This insight also shows the analytical procedure of the optical phase recovery to be applied. As it is well known in the stationary phase approximation of the CWT (see [4] and references therein), the tracking of the local maxima of $|S(a,\mathbf{b})|$ allows the specification of a particular set of data in the space-frequency domain, namely, the ridge a_r, that has the property to describe the spatial evolution of the phase distribution as $\phi(\mathbf{b})=\arctan\{\mathrm{Im}[S(a_r,\mathbf{b})]/\mathrm{Re}[S(a_r,\mathbf{b})]\}$, where Im[ ] and Re[ ] mean the imaginary and real parts, respectively. Note that this procedure was adopted by the CWT in stationary phase approximation for 1D signals. Finally, as the phase values are wrapped, a 1D phase unwrapping algorithm should be used.

To illustrate the performance of the 3DDWT phase recovery procedure, we analyzed simulated TSPI data produced by an out-of-plane interferometer by following the procedure reported in [6]. This analysis was performed by introducing a temporal carrier and by generating interferograms having an average speckle size $s=1$, 3, and 5 pixels. The phase corresponding to the simulated dynamic displacement field was selected as $\phi(x,y,t)=\phi_s(x,y)f(t)$, where $\phi_s(x,y)=5(1-x^2)\exp[-x^2-(y+1)^2]-20(x/2-x^3-y^5)\exp(-x^2-y^2)-\exp[-(x+1)^2-y^2]$, with $-3.5\leqslant x,\ y\leqslant 3.5$ discretized in 200×200 pixels, and $f(t)=8\times10^{-3}(t-64)$ with $1\leqslant t\leqslant 512$, $t\in\mathbb{N}$, where $\mathbb{N}$ denotes the set of natural numbers. The edges of the TSPI data were used in the calculus and removed from the results, being the effective region of the evaluation: $32\leqslant n_x,\ n_y\leqslant 168$ and $64\leqslant t_n\leqslant 448$. Figure 1(a) shows the selected phase distribution $\phi(n_x,n_y,t_n)$ corresponding to the maximum deformation ($t_n=448$). Note that the phase distribution is a linear function of time, and its minimum deformation corresponds to a plane surface ($t_n=64$). To simulate the modulation loss and noise, a random variable with a uniform distribution in $[-\pi/10,\pi/10]$ was added in the phase generation of the TSPI data. We also introduced in the TSPI data five blocks of zeros: A, B, C, D, and E, with dimensions $\Delta n_x=\Delta n_y=15$ and $\Delta t_n=33$ (7425 adjacent null pixels), temporally centered in $t_n=256$ and spatially centered in the local maxima and minima of the phase ϕ. These blocks simulated the sets of adjacent nonmodulated pixels. Figure 1(b) illustrates the spatial distribution of the blocks in the frame $t_n=256$ in the case of a time series of speckle interferograms having an average speckle size of 3 pixels. As a typical example, Fig. 1(c) shows the temporal evolution of the modulation intensity corresponding to the pixel (93, 88) belonging to the block C.

The 3DDWT was computationally implemented as a convolution product in the Fourier space. The tracking of the local maxima of $|S|$ was carried out by using a common computational routine. The phase distribution was retrieved using the arctan equation, and finally a conventional 1D unwrapping method along the time axis was applied. We explicitly ex-

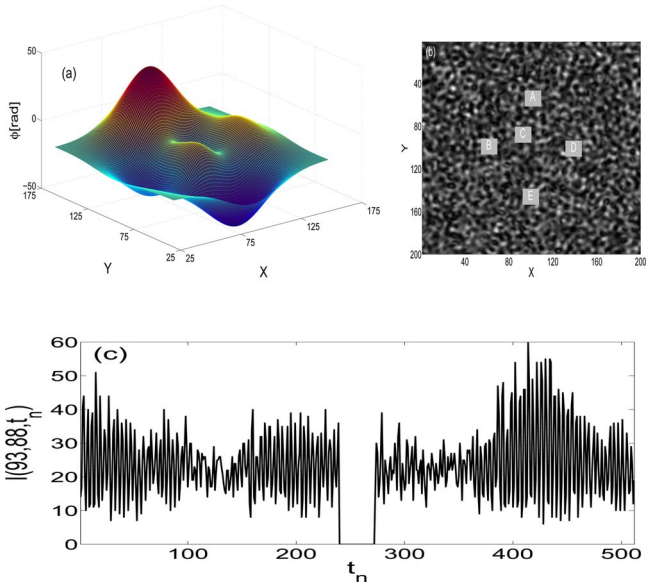

Fig. 1. (Color online) (a) Simulated phase distribution corresponding to the maximum deformation, (b) spatial distribution of the zero blocks in the frame $t_n=256$ when $s=3$ pixels, (c) evolution of the temporal intensity for a pixel belonging to the block C.

cluded the application of robust procedures in the tracking of local maxima and phase unwrapping.

To evaluate quantitatively the retrieved phase distributions, we used a quality index $Q(t_n)$ calculated at each temporal frame and defined by [10,11]

$$Q = \frac{\sigma_{EO}}{\sigma_E \sigma_O} \frac{2\langle E\rangle\langle O\rangle}{\langle E\rangle^2 + \langle O\rangle^2} \frac{2\sigma_E\sigma_O}{\sigma_E^2 + \sigma_O^2}, \tag{4}$$

where O and E are the original phase distribution and the recovered phase, respectively; $\langle\ \rangle$ is the mean value; and σ is the standard deviation. Q has a dynamic range of $[-1,1]$ and allows to model any distortion as a product of three different factors: loss of correlation, luminance distortion, and contrast distortion. We measured the statistical features of each frame $\phi(t_n)$ by combining the three mentioned factors within local regions using a sliding window with a size 7×7 pixels. Figure 2(a) shows the temporal evolution of the quality index for the recovered phase obtained when $s=1$, 3, and 5 pixels, with and without the application of a common smoothing procedure to remove the typical outliers produced in the phase recovery process. The lines with squares, rhombuses, and upright triangles represent the Q values obtained for $s=1$, 3, and 5 pixels, respectively. These results were obtained considering the presence of outliers and by using the parameters of anisotropy $\sigma_t=6$, with $\sigma_x=\sigma_y=0.1$, $\sigma_x=\sigma_y=0.4$, and $\sigma_x=\sigma_y=0.8$, for $s=1$, 3, and 5 pixels, respectively. The scale parameter a was varied in the range [2,7] with steps $\Delta a=0.15$. The lines with dashes, circles, and inverted triangles represent the Q values obtained using a smoothing procedure when $s=1$, 3, and 5 pixels, respectively. Figure 2(b) illustrates the recovered phase distribution obtained at the maximum deformation when $s=3$ pixels and the smoothing procedure was applied. Note that in the case shown in Fig. 2(b), the outliers were easily removed and the Q values were also increased.

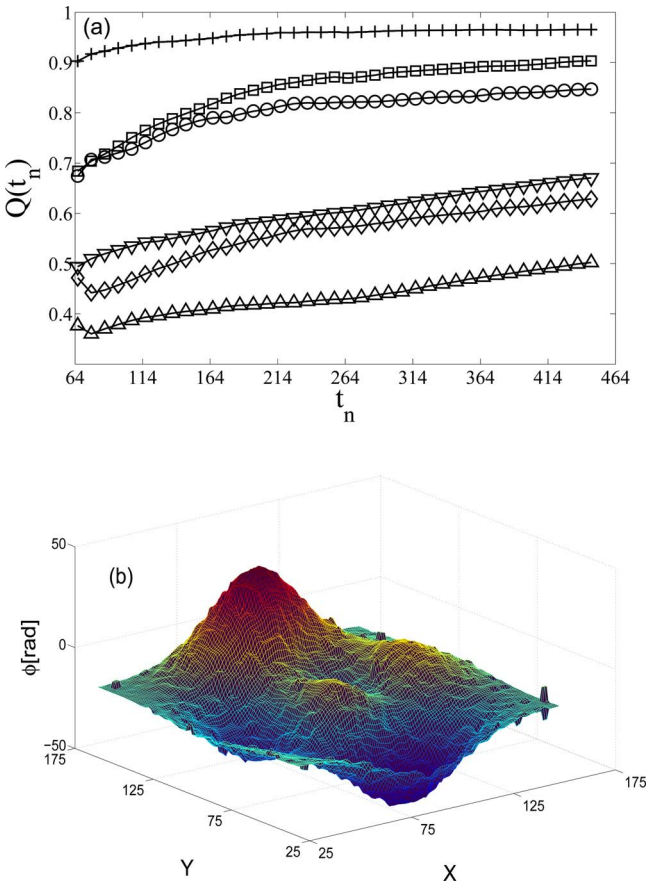

Fig. 2. (Color online) (a) Temporal evolution of the quality index with squares, rhombuses, and upright triangles corresponding to $s=1$, 3, and 5 pixels without smoothing and with dashes, circles, and inverted triangles corresponding to $s=1$, 3, and 5 pixels with smoothing, respectively. (b) Retrieved phase distribution at the maximum deformation obtained with smoothing when $s=3$ pixels.

An additional evaluation was carried out considering the integration effect produced by the CCD detector with three and five speckles per pixel. The obtained results showed greater sensitivity to the introduction of the blocks of zeros than those found in the condition of resolved speckle for the same values of the anisotropy parameters.

To conclude, it is shown that the 3DDWT approach proposed here is a very efficient technique to retrieve phase distributions in TSPI when a significant number of sets of adjacent nonmodulated pixels are present in the recorded data. The 3DDWT is a very useful tool and can retrieve phase distributions with good accuracy where the classical 1D methods fail. The computational complexity of the 3DDWT method lies in the memory requirements, and its digital implementation is fast. New insights and a full evaluation of this phase retrieval method will be presented in a future paper.

The authors are grateful to one of the reviewers of the paper for many useful comments that have helped to improve its understanding.

References

1. J. M. Huntley, in *Digital Speckle Pattern Interferometry and Related Techniques*, P. K. Rastogi, ed. (Wiley, 2001), pp. 59–139.
2. C. J. Tay and Y. Fu, Opt. Lett. **30**, 2873 (2005).
3. Y. Fu, C. J. Tay, C. Quan, and H. Miao, Appl. Opt. **44**, 959 (2005).
4. L. R. Watkins, Opt. Lasers Eng. **45**, 298 (2007).
5. Y. Fu, R. M. Groves, G. Pedrini, and W. Osten, Appl. Opt. **46**, 8645 (2007).
6. F. A. Marengo Rodriguez, A. Federico, and G. H. Kaufmann, Appl. Opt. **47**, 1310 (2008).
7. A. Federico and G. H. Kaufmann, Opt. Lett. **33**, 866 (2008).
8. S. Equis and P. Jacquot, Opt. Express **17**, 611 (2009).
9. R. Murenzi, in *Wavelets, Time-Frequency Methods and Phase Space*, J.-M. Combes, A. Grossman, and Ph. Tchamitchian, eds. (Springer, 1989), pp. 239–246.
10. Z. Wang and A. C. Bovik, IEEE Signal Process. Lett. **9**, 81 (2002).
11. Efficient Matlab implementation and analyzed examples, http://www.cns.nyu.edu/~zwang.